

14. Design of large underground caverns – a case history based on the Mingtan Pumped Storage Project in Taiwan

Introduction

Large underground caverns are used for a variety of purposes in civil engineering. These include caverns housing turbines, electrical generators and transformers in hydroelectric projects, caverns for storing liquid or gaseous fuels, underground warehouses, and underground sports facilities. Because of the high capital costs and the risks associated with public access to these facilities, care must be taken in the design of the caverns to ensure that potential risks are kept to an absolute minimum while, at the same time, providing cost effective and practical engineering solutions. An example of a large underground hydroelectric complex in Taiwan will be used to illustrate the design and process for this type of civil engineering facility and for permanent mining structures such as underground crusher stations.

The Mingtan Pumped Storage Project is located at the geographic centre of Taiwan as illustrated in Figure 1. It utilises the existing Sun Moon Lake as its upper reservoir. The lower reservoir was created by a 60 m high concrete gravity dam on the Shuili River. As illustrated in Figure 2, a pair of 3 km long, 7.5 m diameter headrace tunnels bring the water from the Sun Moon Lake to the surge shafts. From there, inclined steel-lined penstocks convey the water to six reversible pump-turbines, which are housed in a 22 m wide x 46 m high x 158 m long underground power cavern. The transformers are in a parallel 13 m wide x 20 m high x 170 m long cavern. The powerhouse and transformer complex has been excavated in the left bank of the Shuili River at a depth of approximately 300 m below surface. The total generating capacity of the scheme is 1600 megawatts.

The project is owned and operated by the Taiwan Power Company and the engineering design was carried out by Sinotech Engineering Consultants, Inc. Many of the details given below are from papers by Cheng and Liu (1993) and Hoek and Moy (1993).

Geological setting

Taiwan is in the Cenozoic Orogenic belt, at the link between the Ryuku Island Arc to the north and the Philippines Orogeny to the south. It is situated on a convergent and compressive boundary between the Eurasian Plate and the Philippines Sea Plate. The frequent occurrence of earthquakes on the island indicates that Taiwan is located in a belt of young tectonic activity. The mountain ranges extend generally in a north-south direction with the highest peak rising more than 3000 m above sea level. North-south striking thrust faults extend over the entire length of the island.

The Central Range, which forms the backbone of the island, consists of Tertiary sub metamorphic rocks distributed over the western flank and crest, and pre-Tertiary metamorphic rocks distributed over the eastern flank. The Western Foothills are composed of Neogeny clastic sediments in alternating beds of sandstone, siltstone and shale interspersed with limestone and tuff.

The sub metamorphic rocks of the western Central Range (sandstones and argillite) and the sandstones and siltstones of the Western Foothills exhibit tight asymmetric synclines and anticlines, and extensive thrust faulting. The entire area of the project is located between two major north-south faults of this type, namely the Shuilikeng (or Chuchih) fault passing close to the lower reservoir damsite and the Lishan fault running through to the east of the Sun Moon Lake, the upper reservoir of the project.

The power cavern complex is in sandstone, sandstone with siltstone interbeds and several siltstone beds belonging to the Waichecheng Series. The sandstones are fine grained to conglomeratic and sometimes quartzitic. In general, they are strong to very strong although they are slightly to moderately weathered. Locally, softer zones of highly weathered or altered material are encountered. The siltstones are moderately strong and almost always sheared. Occasionally, massive sandstone beds occur with a thickness of up to 7 m. The general appearance of the rock mass in an exploration adit is shown in Figure 3.



Figure 1: Map of the island of Taiwan with the location of the Mingtan Pumped Storage Project in the centre of the country (yellow arrow).

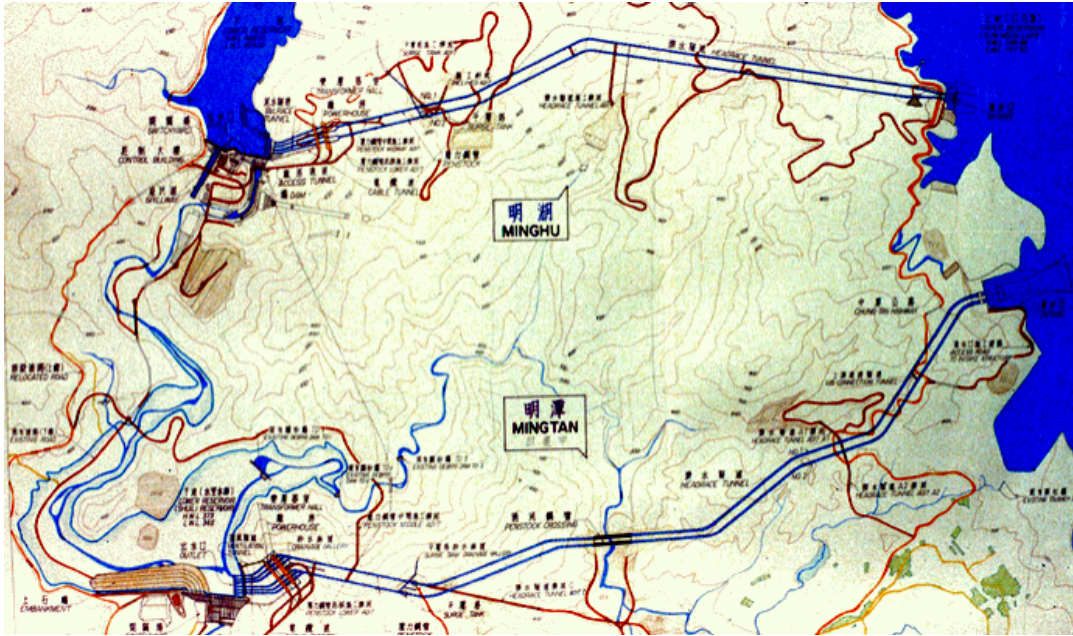


Figure 2: Plan showing the layout of the Minghu Pumped Storage Project (top) and Mingtan Pumped Storage Project (bottom).



Figure 3: Sandstone and siltstone sequence exposed in and underground exploration adit. A thick bed of massive sandstone can be seen in the centre of the photograph and this is sandwiched between bedded sandstones and siltstones of moderate quality. The contact surfaces between these different beds are frequently heavily sheared.

Structural Geology

The attitude of the bedding planes is uniform throughout the powerhouse area, with a strike and dip of N39°E / 34°SE as shown in Figure 4. The bedding is generally tight and spaced from a few centimetres to more than 2 m. Some planes contain a thin layer of clay of about 5 mm thickness.

Eight shear zones (sometimes also referred to as faults) were encountered in the cavern area. All these features are parallel to the bedding planes, occurring in the relatively soft siltstone or interbedded sandstone and siltstone layers. These shear zones are composed of multiple clay seams and shattered, softened, or decomposed rock.

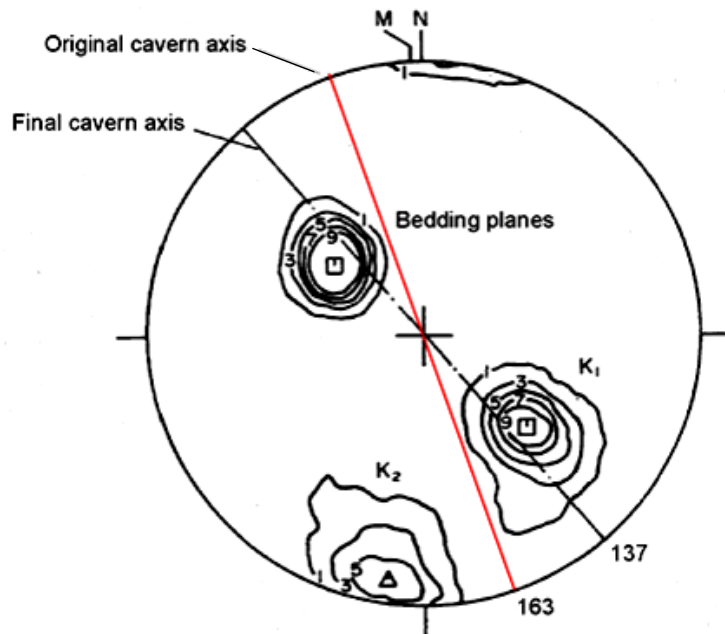


Figure 4: Attitude of bedding planes and joint sets K1 and K2. (based on 2257 measurements)

The original orientation of the power cavern complex, shown in Figure 4, was chosen to keep the penstocks and tailrace tunnels in a straight line. Because of concerns about the formation of wedges in the roof, sidewalls and end walls of the underground caverns, the underground complex was rotated by 26° so that the strike of the bedding planes is almost exactly perpendicular to the cavern axis. While this involved the introduction of curvature in the water transmission tunnels, this curvature was acceptable in view of the improved stability conditions associated with the new alignment.

A geological plan of the powerhouse area is shown in Figure 5 and an isometric drawing of the underground complex is reproduced in Figure 6.

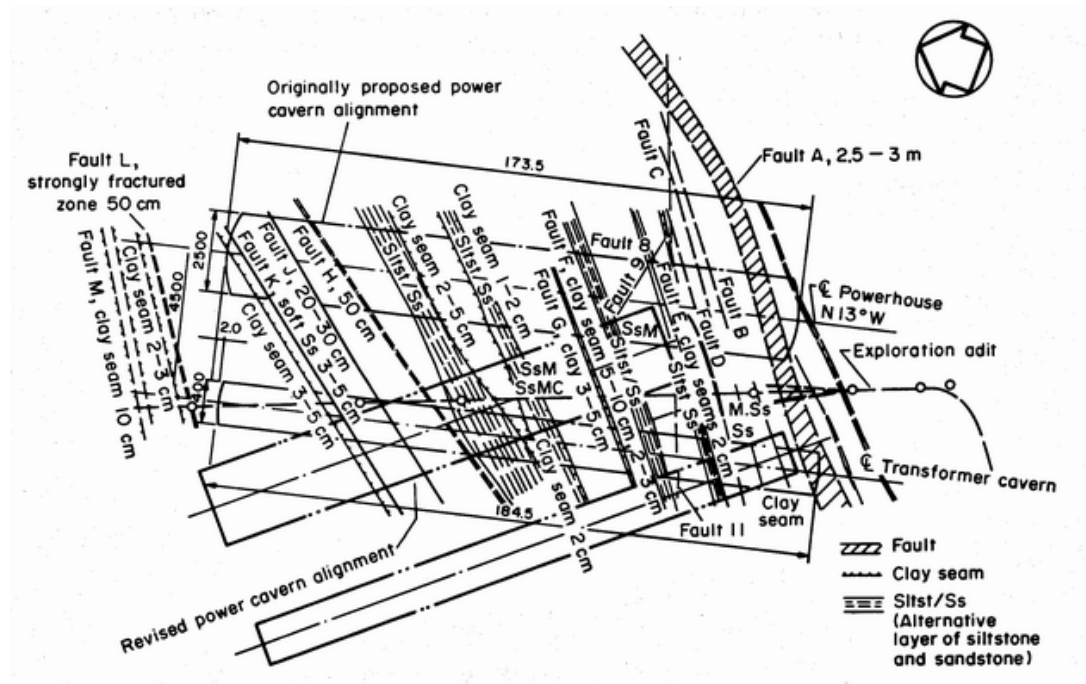


Figure 5: Geological plan of the cavern area showing the original and revised cavern orientations.

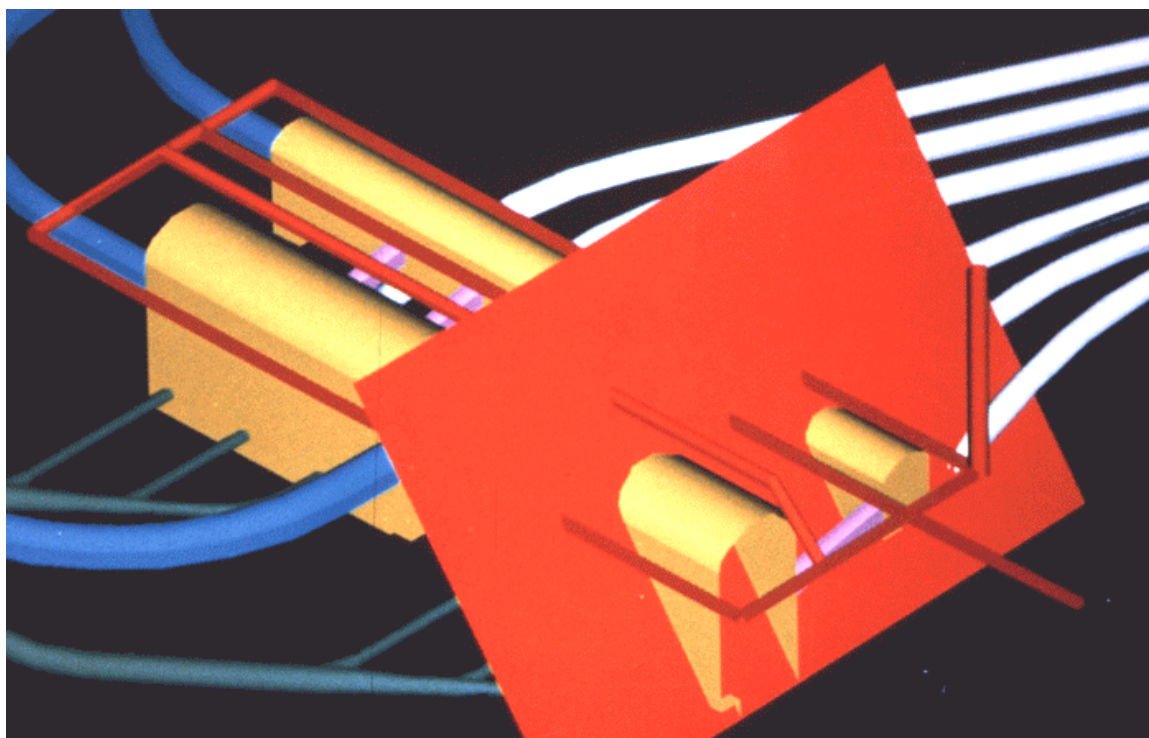


Figure 6: Isometric drawing of the underground complex in relation to the bedding plane orientation (a typical bedding plane is shown in red).

Rock mass properties

Laboratory and in situ tests were carried out in the 1970s for both the Minghu and Mingtan Projects (see Figure 2). The Minghu project was completed in the early 1980s. Detailed design of the Mingtan project commenced in 1982.

The rock mass in the powerhouse area was divided into three types: jointed sandstone, bedded sandstone and faults. The rock mass classifications for these three rock types are given in Table 1. The properties of the intact rock components are listed in Table 2 and the measured in situ deformation modulus values for the rock mass are listed in Table 3. A typical field plate loading test is illustrated in Figure 7.

Table 1: Rock mass classifications for the rock mass in the powerhouse area

<i>Rock type</i>	<i>RMR</i>	<i>Q</i>	<i>Rock quality</i>
Jointed sandstone	63 – 75	12 – 39	Good
Bedded sandstone	56 – 60	7 – 13	Fair to good
Faults or shear zones	10 - 33	0.1 – 1.1	Very poor to poor

Table 2: Intact rock properties from laboratory tests

<i>Rock type</i>	<i>Uniaxial compressive Strength MPa</i>		<i>Modulus of elasticity GPa</i>	
	<i>Range</i>	<i>Average</i>	<i>Range</i>	<i>Average</i>
Sandstone	101-219	166	14.3-29.3	22.3
Siltstone	22-95	41	6.7-16.2	10.6
Interbedded sandstone and siltstone	34-97	66	10.1-17.9	12.8
Coarse grained sandstone	49-123	72		

Table 3: Deformation modulus of rock masses

<i>Rock type</i>	<i>Deformation modulus - GPa</i>	
	<i>Flat jack tests</i>	<i>Plate loading tests</i>
Sandstone	2.7 – 2.9 \perp	3.2 – 5.1 \perp
	2.2 – 5.6 \rightleftarrows	2.3 – 5.0 \rightleftarrows
Siltstone	3.3 – 12.4 \perp	
	5.7 – 14.8 \rightleftarrows	
Interbedded sandstone and siltstone	2.2 \perp	2.8 \perp
	10.9 \rightleftarrows	3.0 \rightleftarrows

\perp Normal to bedding, \rightleftarrows parallel to bedding.



Figure 7: A plate loading test to determine the in-situ deformation modulus of the rock mass exposed in an exploration adit.

On the basis of the rock mass classifications and the laboratory and field tests listed in Tables 1 to 3, the following estimates of the rock mass properties were made using the Hoek-Brown criterion. (Hoek and Brown, 1980, 1988)

Table 4: Estimated rock mass properties – based on laboratory and field tests.

<i>Rock type</i>	<i>RMR</i>	σ_{ci} <i>MPa</i>	m_b	s	c <i>MPa</i>	ϕ <i>degrees</i>	E^1 <i>GPa</i>
Jointed sandstone	63 – 75	100	4.3	0.02	3.8	50	2.7-5.6
Bedded sandstone	56 – 60	100	1.5	0.002	3.3	45	3.3-15
Faults or shear zones	10 - 33	46	0.64	0.0002	0.2	40	2

¹ From in situ test results.

In situ stresses

In situ stress measurements were carried out in an exploration adit using overcoring on a Stress Tensor Tube developed by Rocha et al (1974). The results of these stress measurements are given in Table 5.

Table 5: Measured in situ stresses

<i>Principal stresses</i>	<i>Stress directions</i>	
	<i>Bearing (degrees)</i>	<i>Plunge (degrees)</i>
<i>MPa</i>		
7.1	340	40
3.9	240	10
2.9	140	50

In transforming these stresses onto a plane corresponding to a cross-section of the cavern, a vertical stress of approximately 5.0 MPa is calculated and the ratio of horizontal to vertical stress is found to be approximately 0.9. This compares with the measured ratio of horizontal to vertical stress of 1.4 for the Minghu Power Cavern which is located approximately three kilometres away and which was completed in the early 1980s. In applying these results to the analysis of the Mingtan Power Cavern, a range of horizontal to vertical in situ stress ratios of 0.8 to 1.5 were used to cover the uncertainty associated with the measured value. A further discussion on the interpretation of these in situ stress measurements can be found in Wittke (1990, page 935).

Choice of power cavern shape

The Minghu power cavern was designed by a Japanese consulting group who followed traditional methods involving the use of a cast-in-place concrete arch for supporting the cavern roof. During construction of this cavern very high stresses were induced in both the concrete and the reinforcing steel because of the response of the stiff concrete arch to deformations in the relatively deformable rock mass.

Since the designers of the Mingtan project did not want the same problems to occur in this project, three different cavern shapes were investigated. These cavern shapes were:

- A mushroom shaped cavern with a concrete arch, like the Minghu cavern
- A conventional horseshoe-shaped cavern with vertical sidewalls and
- An elliptical cavern designed for optimal stress distribution in the surrounding rock mass.

The mushroom-shaped cavern was included for reference purposes since the behaviour of the Minghu cavern had been well documented. The conventional horseshoe-shaped cavern was the preferred choice in terms of ease of construction but the elliptical cavern, proposed by a German consulting group, was also analysed. The results of analyses of these three cavern shapes are presented in Figures 8, 9 and 10.

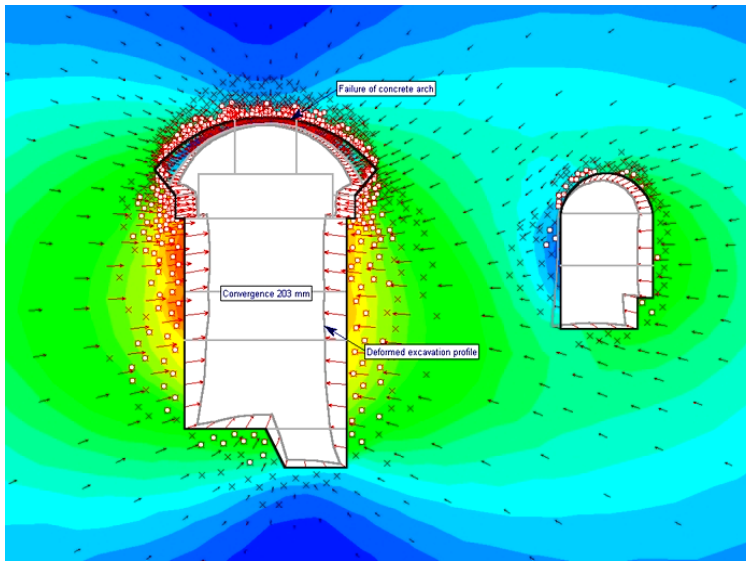


Figure 8: Deformation and failure of the rock mass surrounding a mushroom shaped cavern with a concrete roof arch. Failure of the concrete arch means that this design is not acceptable.

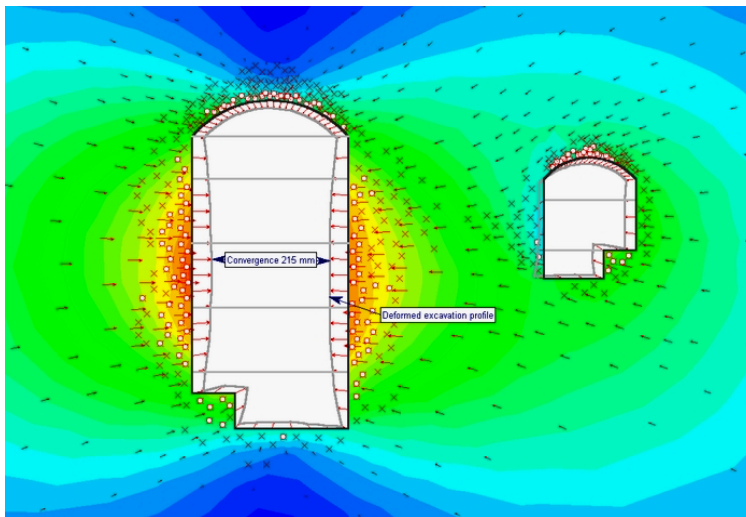


Figure 9: Deformation and failure of the rock mass around an unsupported horseshoe shaped cavern. Failure of the rock mass in the roof and sidewalls is such that extensive support will be required.

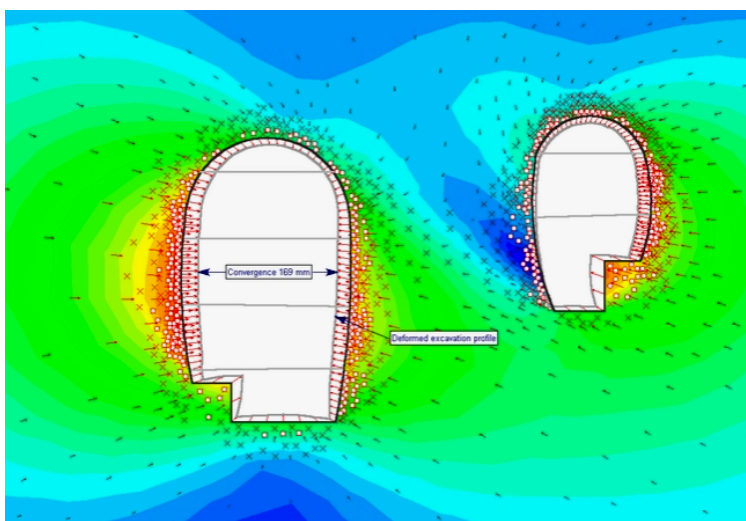


Figure 10: Deformation and failure of the rock mass surrounding an unsupported elliptical cavern. Failure of the rock mass in the roof and sidewalls is such that extensive support will be required, although less than for the horseshoe-shaped cavern.

The comparative studies illustrated in Figures 8, 9 and 10, showed that the mushroom shaped cavern with the concrete roof arch was not an acceptable design. The analysis indicated that even more extensive overstressing of the concrete arch would occur than had been the case in the Minghu cavern. The best stress distribution was given by the elliptical cavern, but it was judged that the amount of support required to stabilise this and the horseshoe shaped cavern would not be significantly different. Consequently, the conventional horseshoe shaped vertical cavern was chosen for the final shape. It was considered that this would make for the simplest construction procedure and that the overall underground complex would incur lower costs than an elliptical cavern.

Distance between caverns

The analyses presented in Figures 8, 9 and 10 show the typical deformation pattern in which the smaller transformer gallery tends to be drawn towards the larger machine hall. This is not a problem when the pillar between these two caverns is sufficiently large but, if the pillar is too small, overstressing of the pillar can occur.

A study was carried out in which the width of the pillar between the transformer gallery and the machine hall was varied. The results of this study showed that the optimum pillar width is obtained when the distance between the two caverns is approximately equal to the height of the larger of the two caverns. This finding is generally applicable when designing caverns in weak rock masses.

Seam treatment in the cavern roof

The final layout of the Mingtan powerhouse and transformer caverns is illustrated in Figure 11. The project was constructed in two phases such that preparatory works were carried out in a preliminary contract, while the bulk of the construction was carried out in the main contract. This arrangement provided the opportunity for stabilization of the cavern roof to be carried out during the preliminary contract.

As pointed out earlier and as illustrated in Figure 5, the powerhouse cavern crosses eight faults or shear zones. The influence of these faults on the stability of the cavern was of major concern and it was decided that pre-treatment of the cavern roof was necessary in order to ensure that the main contract could proceed without severe problems due to roof instability. This pre-treatment consisted of removal and replacement of the clay seams in the faults to the maximum extent possible, followed by reinforcement of the rock mass in the roof by means of grouted cables.

The treatment of the faults involved high pressure washing of the clay seams and backfilling the voids with non-shrinking concrete. This technique was developed for the treatment of similar faults in the foundation of the Feitsui arch dam near Taipei (Cheng, 1987). Figure 12 shows the arrangement of longitudinal working galleries and cross-cuts used to access the clay seams. It was found that the clay washing, and replacement could be carried out to a depth of about 4 m. The thickest and weakest fault (Fault H in Figure 5) was manually excavated and backfilled to a similar depth.

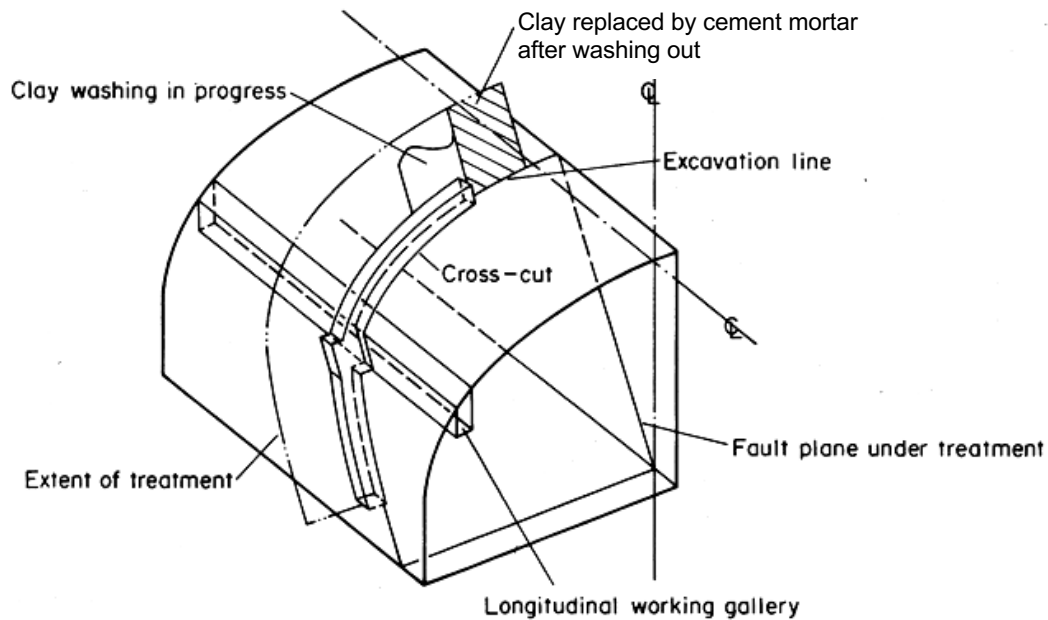


Figure 12: Washing and replacement of clay seams in the faults encountered in the roof and upper sidewalls of the Mingtan power cavern. This treatment was carried out from two longitudinal working galleries before excavation of the cavern commenced in the main contract.

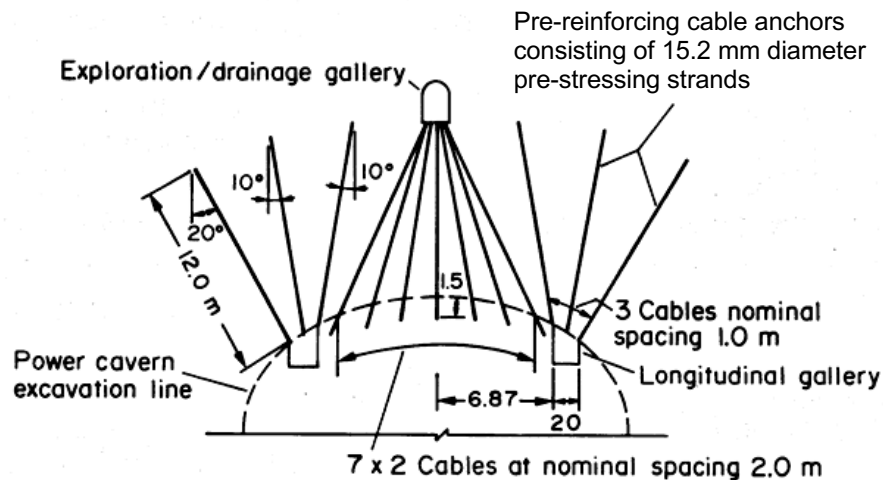


Figure 13: Pre-reinforcement of the power cavern roof by means of grouted untensioned cables placed from the longitudinal working galleries and from an existing exploration and drainage gallery above the roof.

Once the seam treatment in the roof had been completed, a series of untensioned grouted cables were installed as illustrated in Figure 13. Since these cables were installed before excavation of the cavern commenced, tensioning of the reinforcement was not necessary since the cables would be loaded by deformation induced by the cavern excavation. A load of a few tons was used to straighten the cables before they were fully grouted in place. As the lower ends of the cables installed downwards from the drainage gallery were exposed in the roof of the cavern, these ends were cleaned, and an anchor system was installed before the excess cables lengths were cut off.

The installation of the cables from one of the longitudinal working galleries is illustrated in Figure 14.



Figure 14: Untensioned grouted cables installed from the longitudinal working galleries to pre-reinforce the rock mass above the power cavern roof.

Choice of cavern roof and sidewall reinforcement

In contrast to the Minghu Powerhouse Cavern in which the roof is supported by a stiff concrete arch, the Mingtan Cavern is supported by “active” support consisting of cables, rockbolts and shotcrete. A precedent for the design of this support is the experience from existing caverns, plotted in Figures 15 and 16.

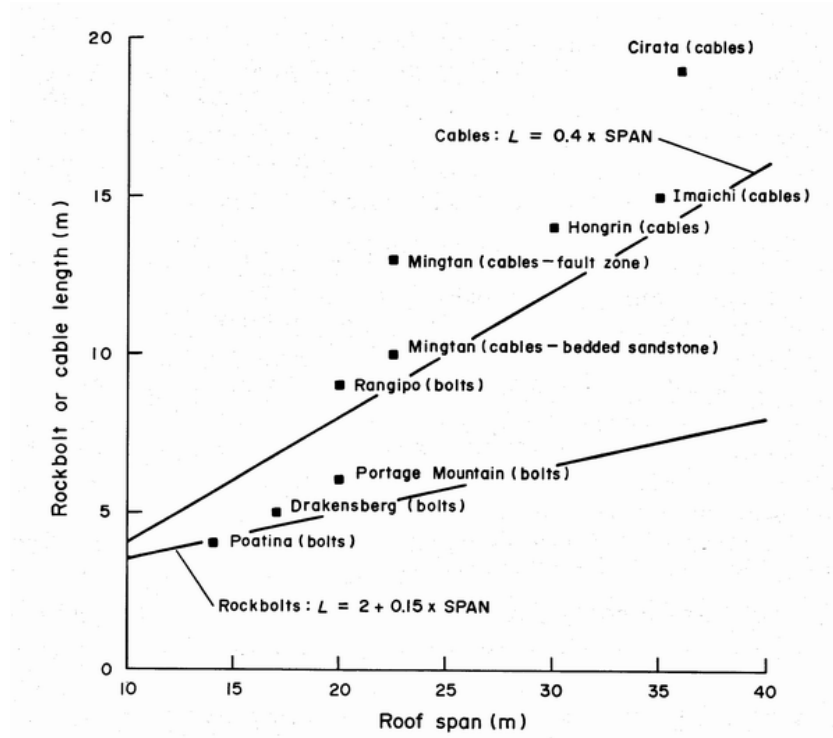


Figure 15: Precedents for rockbolt and cable lengths for different cavern roof spans.

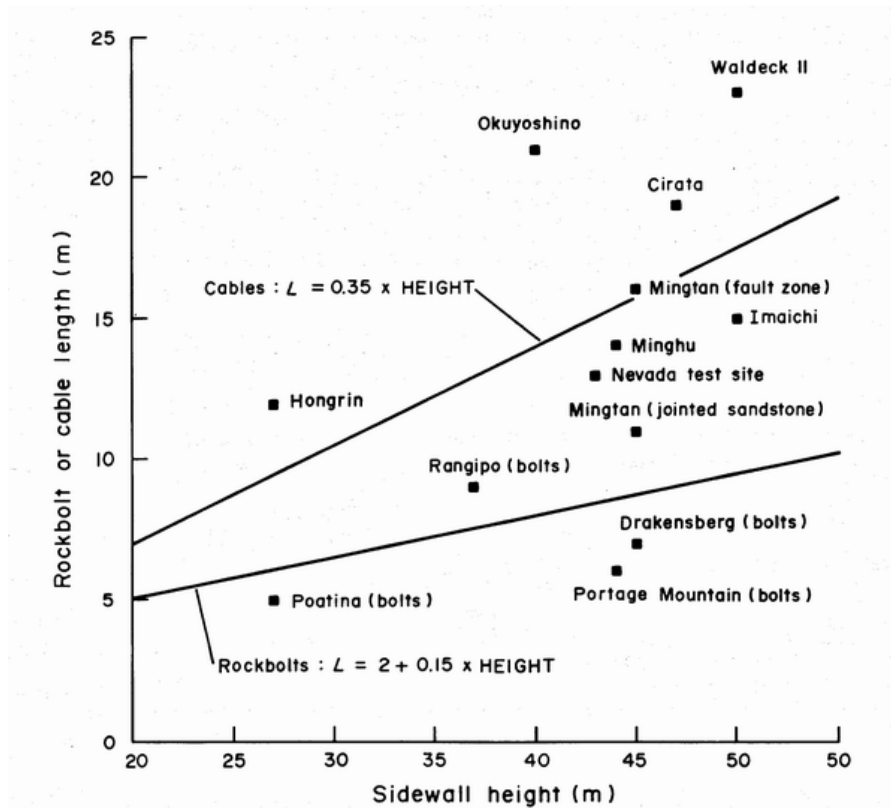


Figure 16: Precedents for rockbolt and cable lengths for different cavern sidewall heights.

Early in the design process it was decided to use cables rather than rockbolts as the primary support system. As can be seen from Figures 15 and 16, the chosen cable lengths were between 10 and 12 m for the roof and 10 and 15 m for the sidewalls of the cavern, depending upon the material in which the cables were anchored. These cable lengths were confirmed and refined by means of the numerical analyses described later.

While shotcrete played an important role in maintaining the integrity of the exposed rock in the cavern roof and sidewalls, its contribution was ignored in designing the overall support system. The decision to ignore the contribution of shotcrete was made on the basis that shotcrete had not been used in any previous cavern construction in Taiwan and it was felt that this lack of experience could lead to shotcrete of uncertain quality and reliability. In fact, this is a prudent step in any cavern design where there is doubt about the control of construction quality. Shotcrete is particularly vulnerable to deficiencies in the skill of the operators. It is not wise to rely on its support effectiveness where construction quality is questionable.

Interactive design using numerical analysis

The main contract for the construction of the Mingtan underground complex was an Owner-Engineer-Contractor Target Price contract in which the Engineer played a very active role during construction. The good-for-construction drawings indicated the construction sequence, the lengths of cables and rockbolts and the thickness of the shotcrete, but included considerable latitude for these items to be varied during construction, depending upon the measured performance of the support elements.

Seven instrumentation stations were set up along the axis of the cavern. These consisted of grouted rod extensometers in the roof and sidewalls as well as cable anchor load cells on selected cables that were left ungrouted. The roof extensometers, illustrated in Figure 17, played a critical role in the interactive design process since these were installed before excavation of the cavern commenced and they provided a calibration of the assumed rock mass properties used in the numerical models.

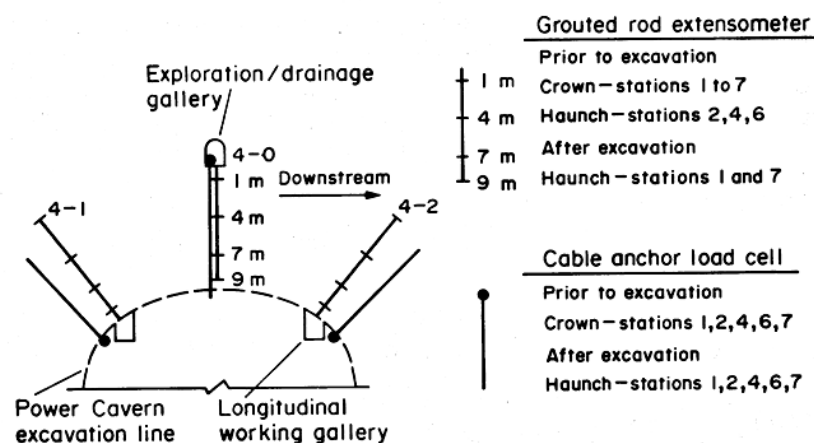


Figure 17: Typical instrumentation array installed in the cavern roof before excavation of the cavern commenced.

The two-dimensional finite difference Itasca program FLAC was the primary tool used for back-analysis of the measured response of the rock mass above the roof of the cavern and for analysis of the remaining support system.

When construction of the cavern commenced, the deformations in the roof were measured by means of the extensometers illustrated in Figure 17. These deformations were compared with those predicted by the numerical modelling. It was found that the deformations in the immediate vicinity of the roof were significantly greater than predicted. Therefore, it was necessary to reduce the modulus of the rock mass in this region by a factor of almost 2 in order to bring the predicted and measured values into coincidence. It was concluded that this modulus reduction was due to blast damage and, for the remaining numerical models, a 2 m thick zone of “blast damaged” rock was wrapped around each excavation stage.

The properties of the rock mass and blast damaged zone, derived from back analysis of the cavern arch excavation, are listed in Table 6. Comparing these properties with those listed in Table 4 shows a reasonable agreement although the cohesive strengths are generally lower than those predicted from the laboratory tests.

Table 6: Rock mass properties derived from back-analysis of cavern arch excavation.

<i>Rock type</i>	<i>c</i> <i>MPa</i>	<i>φ</i> <i>degrees</i>	<i>E</i> <i>GPa</i>
Jointed sandstone	1.0	50	6.0
Bedded sandstone	0.8	45	4.5
Faults or shear zones	0.15	30	2.0
Blast damage zone	0.2	45	2.5

The appearance of the initial blast results in the first section of the cavern to be excavated is illustrated in Figure 18. The dipping bedded sandstone made it very difficult to achieve an accurate excavation profile and loosening of the rock mass immediately behind this profile is inevitable. Figure 19 shows that, as experience was gained, the appearance of the cavern improved significantly.

Typical numerical modelling details are illustrated in Figures 20 and 21. In this case the model has been re-created using the RocScience program, Phase2 rather than FLAC, which was used for the original analysis. This model was excavated in six stages and the cable reinforcement was installed in each stage to simulate the actual construction sequence. This model shows that the rock mass failure (denoted by the × symbol for shear and the ○ symbol for tension) are generally well contained by the envelope of the reinforcing cables. The deformation of the cavern boundary is evenly distributed around the cavern perimeter thereby satisfying one of the key criteria for acceptability of the performance of the support system.



Figure 18: Blast damage in the first section of the cavern arch to be excavated.



Figure 19: Completed excavation of the cavern arch.

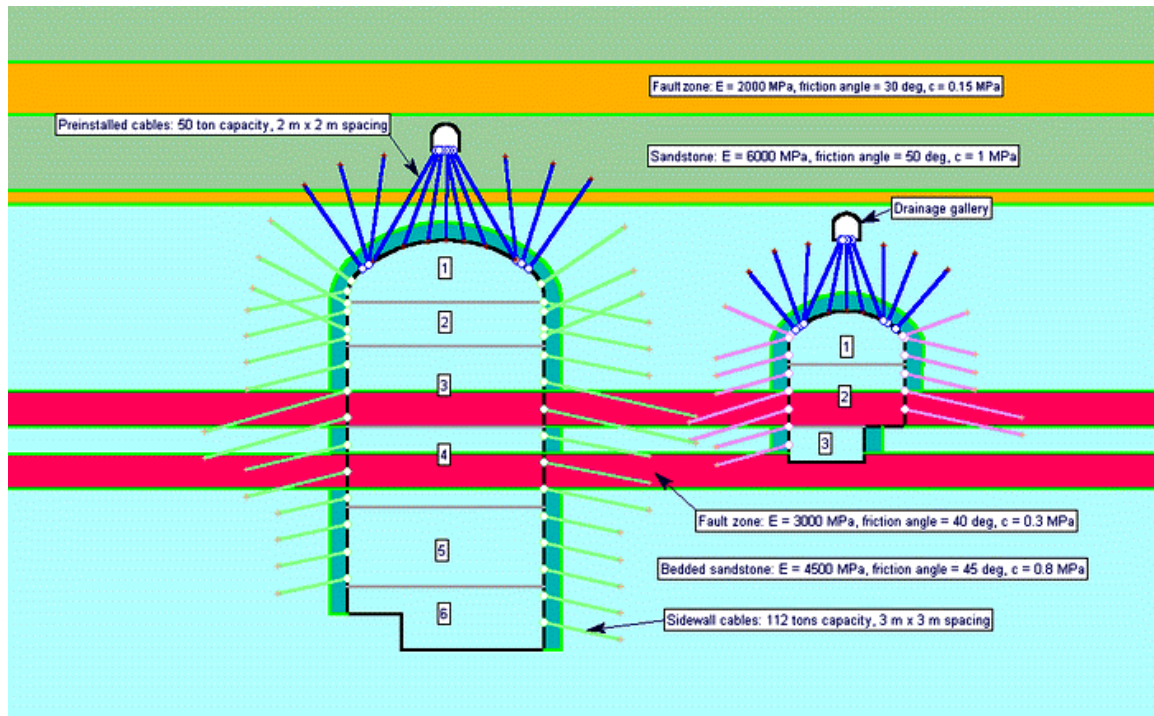


Figure 20: Numerical model showing distribution of material and layout of reinforcement in the rock mass surrounding the caverns.

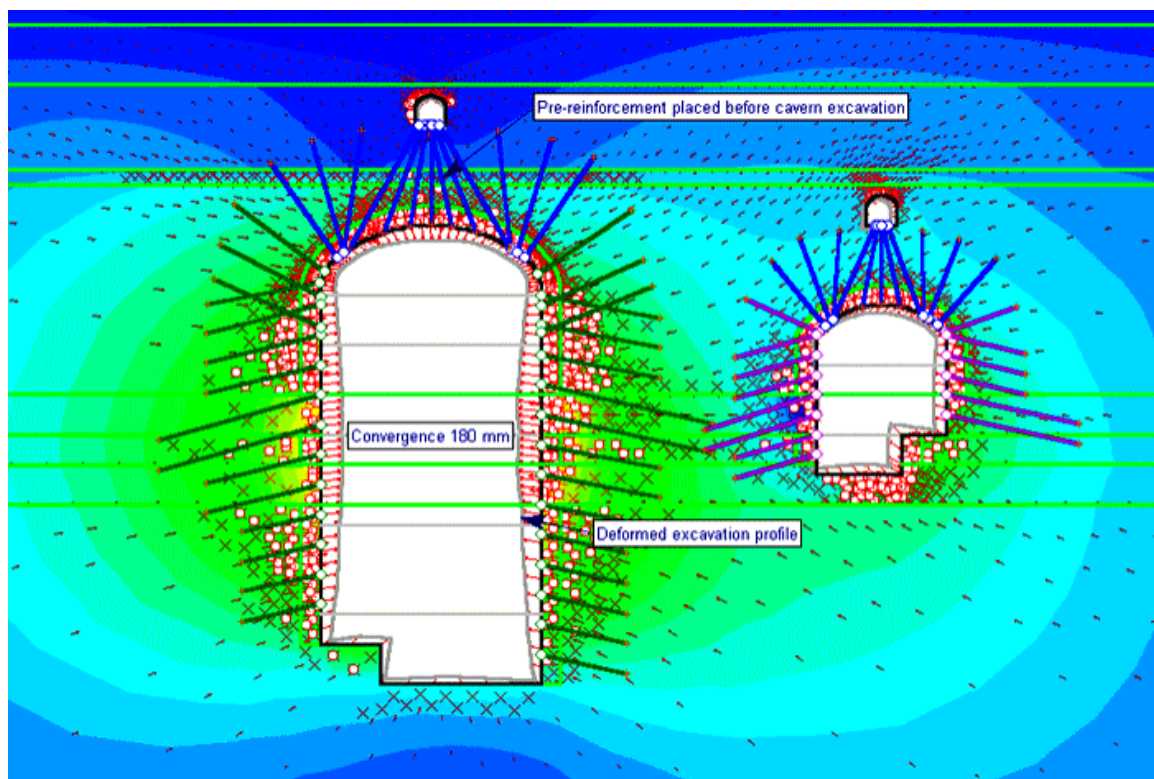


Figure 21: Typical results from numerical modelling showing rock mass failure and deformation of the cavern boundaries.

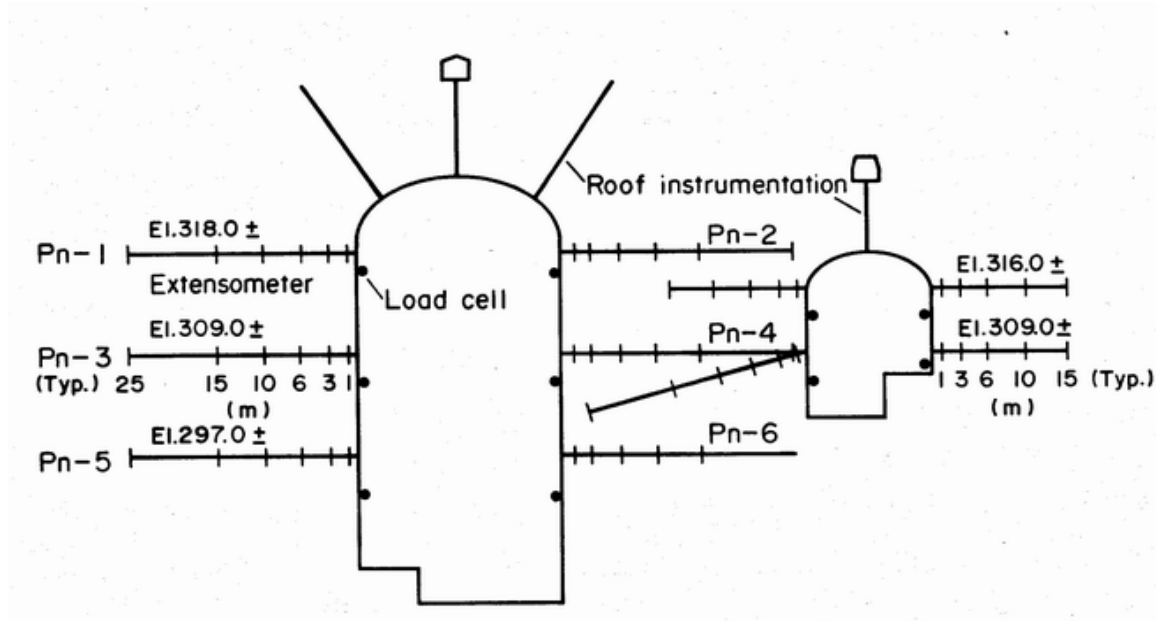


Figure 22: Typical layout of sidewall extensometers for the Mingtan underground complex.

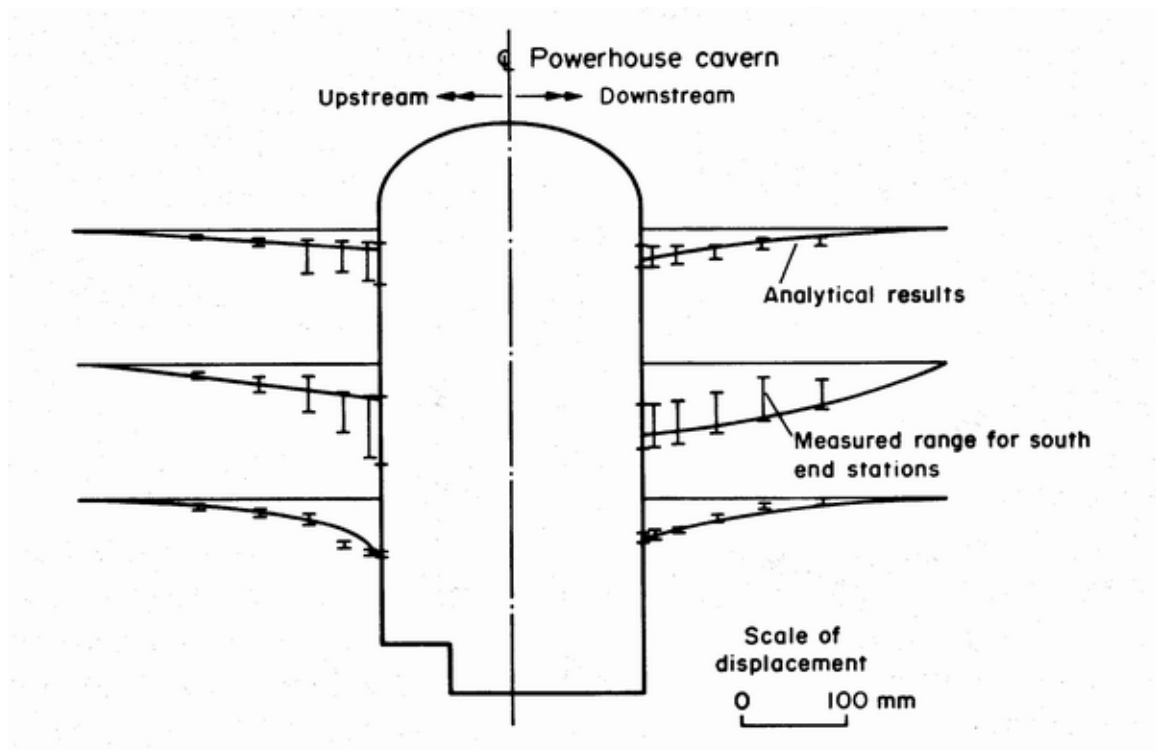


Figure 23: Comparison between predicted and measured deformations in the Mingtan Power Cavern sidewalls.

The layout of the extensometers in the cavern sidewalls is illustrated in Figure 22 while Figure 23 shows a comparison between the measured and predicted sidewall deformations. In general, the agreement between the measured and predicted deformations for all seven measuring stations along the cavern was very good. The use of the numerical model proved to be a very powerful tool in ongoing refinement of the cavern support design as construction progressed.

Details of the cables installed in the roof and sidewalls of the Mingtan Powerhouse Cavern are given in Figure 24.

Temporary crane beam design

A critical factor in the design of any large cavern is the availability of cranes to assist in the various stages of construction. When the cavern roof is supported by means of rockbolts or cables and shotcrete, it is particularly important to maintain access to the roof at all stages. This is necessary because the shotcrete tends to crack due to deformation induced by downward excavation of the cavern. In addition, damage to the rockbolts or cables needs to be repaired, as well, it is sometimes necessary to install additional reinforcement to deal with un-anticipated problems.

In the case of the Mingtan Cavern, extensometer measurements in one part of the cavern roof indicated that excessive movements were occurring. Close inspection of this area revealed that a set of intersecting discontinuities had released a wedge of rock which was not adequately supported. Because this problem was detected in good time, it was remedied by the installation of additional cables in the area. The availability of a crane at this stage of construction was important since it enabled continuous inspection and repair of the cavern roof.

There are various approaches to the provision of cranes in large caverns. In some cases, the temporary construction crane is supported on light rails which are rockbolted to the cavern sidewalls. This was the case for the Mingtan Cavern. The temporary crane rails are shown in Figure 25 which is a view of the cavern from the temporary crane platform. As shown in Figure 11, the permanent crane is supported on rails carried on concrete columns.

Another approach is to combine permanent and temporary crane beams into a single system. This was done for the Drakensberg Pumped Storage Project in South Africa where heavy cast-in-place concrete beams were anchored to the cavern walls as illustrated in Figure 26. These provided support for both the temporary construction crane, illustrated in Figure 27, and for the main cavern crane.

Figure 28 shows the crane beam suspended from the curved sidewalls of an elliptical power cavern in the Singkarak hydro-electric project in Indonesia. A different approach is illustrated in Figure 29 which shows the crane beams for the temporary construction crane in the Thissavros project in Greece. These beams were later supported on concrete columns to provide support for the much heavier main crane.

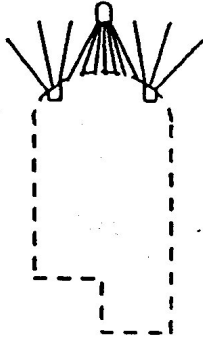
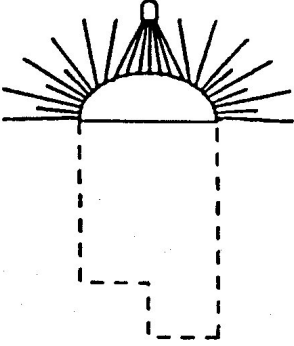
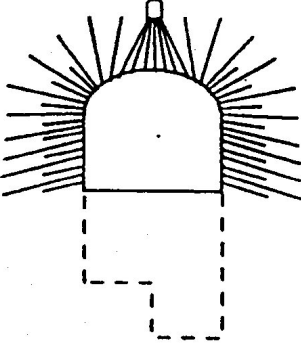
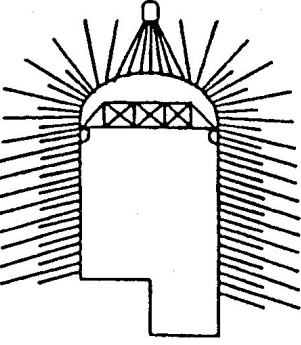
<p>a</p> 	<p>Installation of double corrosion protected cables from exploration/drainage gallery located 10 m above center of roof arch and from two longitudinal working galleries. The 50 tonne capacity cables were installed on a 2 m x 2 m grid pattern and a small straightening load of 5 tonnes was applied before grouting.</p> <p>Dashed lines show cavern profile before excavation.</p>
<p>b</p> 	<p>Excavation of cavern roof by center heading and slashing with application of first 50 mm thick layer of steel fiber reinforced micro-silica shotcrete. Faceplates were added to projecting ends of cables and tensioned to 20% of ultimate capacity to ensure positive anchorage. Where required, 5 m long 25 mm diameter mechanically anchored, tensioned and grouted rockbolts installed at centers of 2 m x 2 m grid of cable reinforcement.</p>
<p>c</p> 	<p>Excavation of cavern by 2.5 m vertical benches. Double corrosion protected 112 tonne cables, inclined downwards at 15° to cross bedding planes, were installed on a 3 m x 3 m grid in the sidewalls. Before grouting, these were tensioned to 38 to 45% of yield strength, depending upon their location relative to the bench. Intermediate 6 m long 25 mm diameter tensioned and grouted rockbolts were installed between cables. Final shotcreting of the roof was carried out at an early stage of benching.</p>
<p>d</p> 	<p>Complete excavation of the cavern with 150 mm total thickness of steel fiber reinforced micro-silica shotcrete on the roof and upper sidewalls and 50 mm thickness on the lower sidewalls. Access to roof for inspection and minor remedial bolting maintained from temporary crane.</p>

Figure 24: Details of cable support installed in the Mingtán Power Cavern.



Figure 25: View of the Mingtan cavern from the platform of a temporary construction crane supported on rails bolted to the cavern walls.



Figure 26: Cast in place concrete crane beam being anchored to the sidewall of the power cavern of the Drakensberg Pumped Storage Project in South Africa.

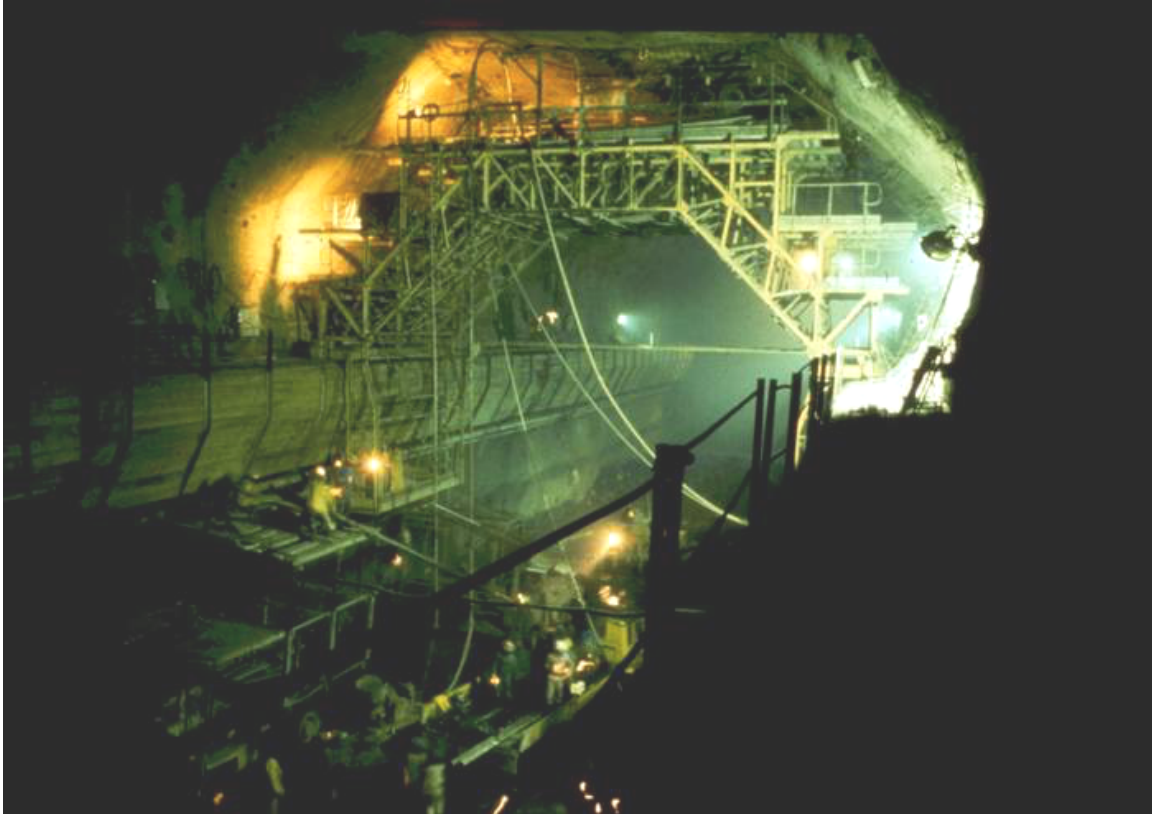


Figure 27: Temporary construction crane running on the main crane beams of the Drakensberg Power Cavern.



Figure 28: Crane beam anchored to the curved wall of the elliptical power cavern of the Singkarak hydroelectric project in Indonesia.



Figure 29: Crane beams rock bolted to the walls of the power cavern of the Thissavros hydroelectric project in Greece. These rails provided support for the temporary construction crane shown in the photograph. The stubs projecting from the bottom of the beams were later attached to concrete columns that provided support for the main crane.

Need for three-dimensional numerical modelling

The design of the Mingtan underground complex was carried out with the aid of two-dimensional numerical models. A few three-dimensional model analyses were carried out, but these were of limited value in this project. On the other hand, in some projects it is important to use three-dimensional models to study critical elements of the design. In particular, the bus tunnels, linking the powerhouse and the transformer caverns and the draft tubes at the base of the power cavern, can create critical construction problems in weak or heavily structured rock masses.

Figure 30 shows a three-dimensional model of the underground complex of the Nathpa Jhakri Hydroelectric Project in India. This model was created using the program 3DEC and was used to investigate the overall stability of the cavern complex in a rock mass in which the properties varied significantly along the length of the complex.

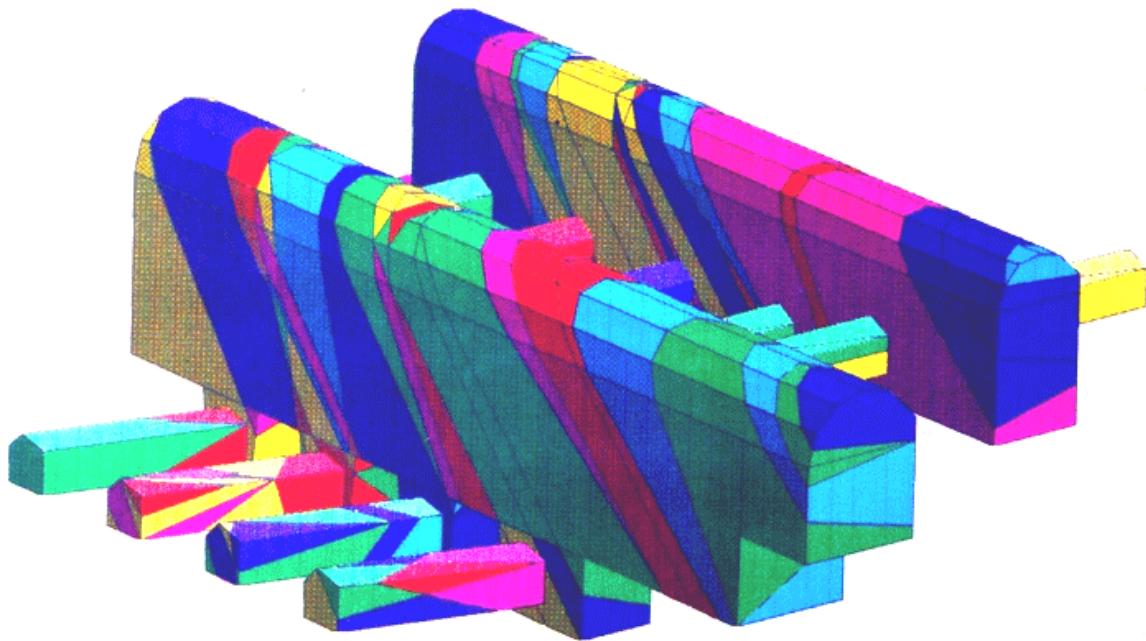


Figure 30: Three-dimensional 3DEC model of the Nathpa Jhakri underground caverns in India. Different colours in the model denote different rock mass properties. The complexity of the intersections of the four draft tubes and the lower part of the cavern can be seen in this illustration. This model study was carried out by Dr B. Dasgupta.

Long-term performance

While the Mingtan support system described earlier performed very well during construction, there was some concern about its long-term performance and its response to possible creep movements in the rock mass. Consequently, monitoring of many of the instrument arrays was continued for several years after construction.

The early part of the monitoring record for the roof and haunch extensometers in the Mingtan power cavern is shown in Figure 31. These curves show rapid response of the extensometers to excavation of the top heading and upper benches. This is followed by stabilisation of the deformations as the cavern is benched down to its lowest elevation.

In the ten years since the project was completed and put into operation, ongoing measurements of some of these instruments has shown that long-term movement of the rock mass is negligible. This confirms typical observations in most rock masses, other than rheological material such as salt and potash, in which excavations, that have been fully stabilised, do not exhibit time dependent behaviour.

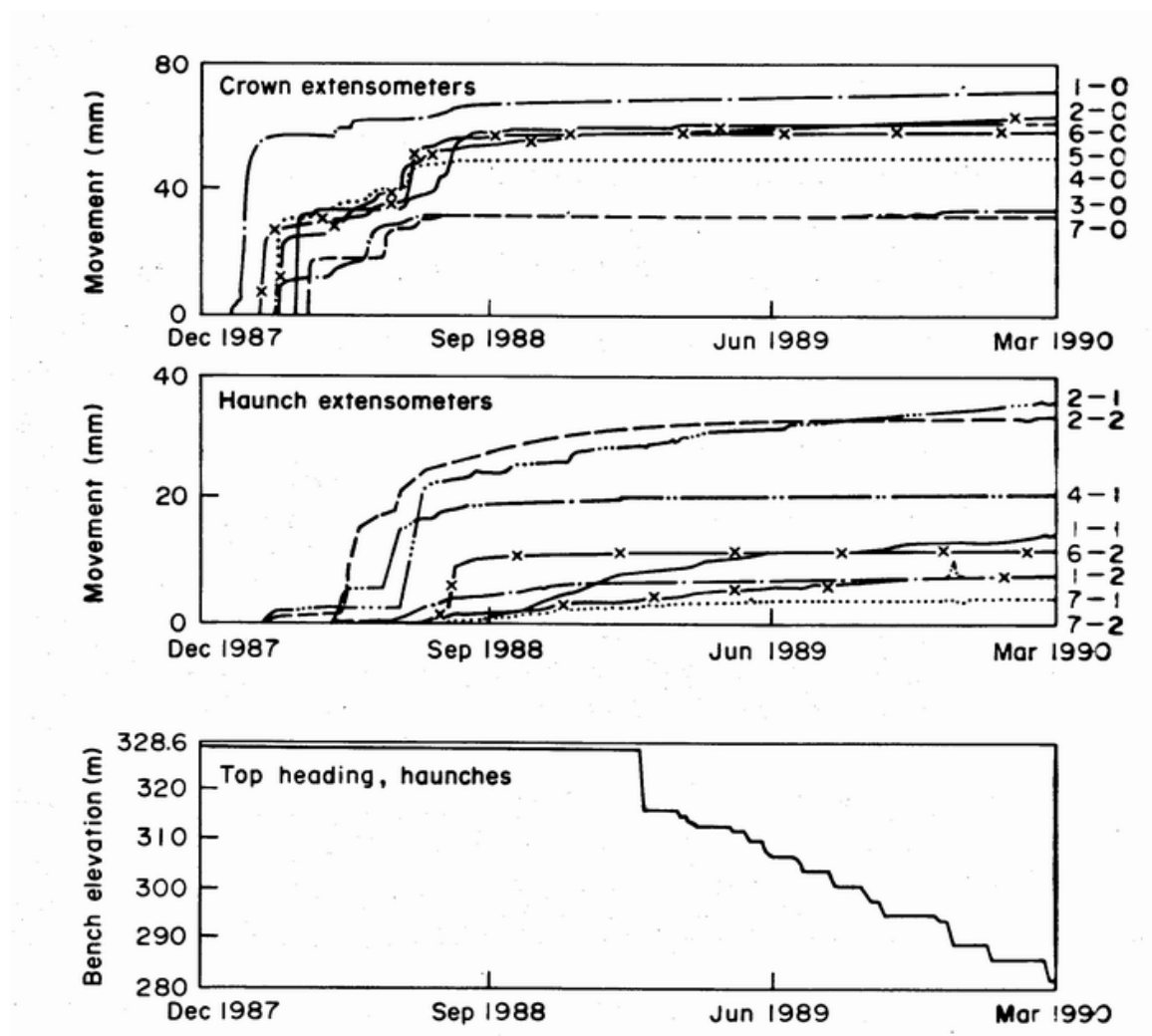


Figure 31: Response of crown and haunch extensometers in the seven monitoring sections along the length of the Mingtan Power Cavern.

The ultimate test – earthquake loading

A Richter magnitude 7.6 earthquake occurred very close to the Sun Moon Lake in the central mountains of Taiwan on September 21, 1999. The epicentre of this earthquake has been placed at approximately 15 km from the Mingtan Project, as illustrated in Figure 32.



Figure 32: Location of the September 21, 1999 Richter magnitude 7.6 earthquake in relation to the Mingtan Project.

In accordance with normal underground cavern design procedures, no allowance had been made for earthquake loading in the design of the Mingtan underground complex. Hence, the loading imposed by the large earthquake of September 21, 1999, represented an ultimate test of the validity of this design approach. Incidentally, it was reported that 98% of the surface buildings were structurally damaged in the town of Puli, close to the earthquake epicentre.

Soon after the earthquake, the Sun Moon Lake area was visited by a team organised by University of California, Berkeley, and funded by the US National Science Foundation. Dr Mike McRae of Jacobs Associates, consulting engineers in El Segundo, California, was a member of this team and his comments on the visit are as follows²:

“We visited Mingtan and Minghu and both facilities exhibited only minor damage. Minghu exhibited some hairline cracks in the sidewalls of the main chamber and several new leaks had developed in the upstream wall of the powerhouse, the largest (about 10 gallons per minute) being in the area of the penstock intersection closest to the control room. Some localised spalling in the granite tiles in the floor of the powerhouse had also occurred. It was also reported to us that the inflows into the drainage gallery had increased.

The results of the instrumentation at Mingtan indicates 5 mm of additional crown displacement following the earthquake and an increase in the water inflow from 0.027 m³/sec to 0.05 m³/sec. During our inspection of the roof of the powerplant we observed some very localised cracking in the shotcrete with the cracks being up to 12 mm wide and up to 2.5 m long. It appears that seismically induced movements in the localized blocks were responsible for the cracking. No significant leaks were observed in the crown. Some minor cracks were also observed in the wall near the control room.”

Acknowledgements

The permission of the Taiwan Power Company and of Sinotech Engineering Consultants Inc., to use the material presented in these notes, is gratefully acknowledged.

References

- Cheng, Y. 1987. New development in seam treatment of Feitsui arch dam foundation. *Proc. 6th cong. ISRM, Montreal*, 319-326.
- Cheng, Y. and Liu, S.C. 1990. Power caverns of the Mingtan Pumped Storage Project, Taiwan. In *Comprehensive Rock Engineering* (ed. J.A. Hudson) **5**, 111-132. Oxford: Pergamon.

² Fax from Mike McRae to Evert Hoek, 14 October 1999.

- Hoek, E. and Brown E.T. 1988. The Hoek-Brown failure criterion - a 1988 update. *Proc. 15th Canadian Rock Mech. Symp.* (ed. J.H. Curran). Toronto: 31-38. Civil Engineering Dept., University of Toronto.
- Hoek, E. and Brown E.T. 1980. *Underground Excavations in Rock*. London: Instn Min.Metall.
- Hoek, E. and Moy, D. 1993. Design of large powerhouse caverns in weak rock. In *Comprehensive Rock Engineering*, (ed. J.A. Hudson) **5**, 85-110. Oxford: Pergamon.
- Rocha, M., Silvério, A., Pedro, J.O. and Delgado, J.S. 1974. A new development of the LNEC stress tensor gauge. *Proc. 3rd ISRM congress, Denver*. **1**.
- Wittke, W. 1990. *Rock Mechanics – Theory and Applications with Case Histories*. Berlin: Springer-Verlag.